Amino Acids (2013) 44:1457–1475
DOI 10.1007/s00726-013-1474-4

INVITED REVIEW

Analysis of DNA interactions using single-molecule force spectroscopy

Markus Ritzefeld · Volker Walhorn · Dario Anselmetti · Norbert Sewald

Received: 30 January 2013 / Accepted: 13 February 2013 / Published online: 7 March 2013

Abstract Protein–DNA interactions are involved in many biochemical pathways and determine the fate of the corresponding cell. Qualitative and quantitative investigations on these recognition and binding processes are of key importance for an improved understanding of biochemical processes and also for systems biology. This review article focusses on atomic force microscopy (AFM)-based single-molecule force spectroscopy and its application to the quantification of forces and binding mechanisms that lead to the formation of protein–DNA complexes. AFM and dynamic force spectroscopy are exciting tools that allow for quantitative analysis of biomolecular interactions. Besides an overview on the method and the most important immobilization approaches, the physical basics of the data evaluation is described. Recent applications of AFM-based force spectroscopy to investigate DNA intercalation, complexes involving DNA aptamers and peptide– and protein–DNA interactions are given.

Keywords AFM · Single-molecule force spectroscopy · DNA · Protein

Introduction

Replication, DNA repair, gene regulation, and transcription are essential cellular processes in all organisms. In order to investigate the involved protein–DNA interactions in a systems biology context it is necessary to quantify and analyze them. Apart from ensemble methods like surface plasmon resonance (SPR) that we recently reviewed (Ritzefeld and Sewald 2012), single-molecule methods are able to accurately analyze and quantify the recognition of DNA sequences by proteins. They facilitate the investigation of the complex relationship between force, lifetime, and chemistry even of low-affinity interactions. Beside techniques like optical tweezers (Ashkin and Dziedzic 1987) and magnetic tweezers (Gosse and Croquette 2002), atomic force microscopy (AFM) is the most prominent approach. In this review article we will first of all recapitulate the basic principle of AFM-based single-molecule force spectroscopy (SMFS). After a short summary of the most prominent immobilization techniques we will explain the basics of the evaluation process. Finally we will summarize how this method has been recently adopted to investigate DNA interactions.

Single-molecule force spectroscopy—the setup

The central part of an AFM is the force sensor, the so-called cantilever, which often is a sharp pyramidal tip attached at the end of a typically hundred micrometer long flexible flat spring (Binnig et al. 1986). Either the cantilever or the surface underneath the tip can be moved very accurately with a piezoelectric 3D-scanner. If the cantilever tip interacts with an analyte immobilized on the surface, a force is imposed that results in the deflection of the cantilever. Commonly, the bending of the cantilever is measured from the displacement of a laser beam that is reflected off the cantilever on a quadrant photodiode detector (Meyer and Amer 1988). The technique enables

M. Ritzefeld · N. Sewald (✉)
Organic and Bioorganic Chemistry, Bielefeld University, Bielefeld, Germany
e-mail: norbert.sewald@uni-bielefeld.de

V. Walhorn · D. Anselmetti
Single Molecule Biophysics, Bielefeld University, Bielefeld, Germany

imaging of a certain analyte in a sub-nanometer resolution even under near-physiological conditions (Drake et al. 1989; Shao et al. 1995). In contrast to the imaging mode, where substances are scanned line by line, the cantilever in an AFM single-molecule force spectroscopy setup is moved only in the vertical direction (cf. Fig. 1a). Immobilizing two interacting substances on the cantilever tip and the surface, respectively, enables the recording of high-resolution force-versus-extension curves (Florin et al. 1994; Lee et al. 1994; Dammer et al. 1995; Smith et al. 1996). An accurately calibrated system enables pN-resolution measurements (Ralston et al. 2005). The small radius of the cantilever tip ($\sim$10 nm) in combination with sparsely distributed binding partners on the sample surface facilitates a high spatial discrimination allowing for the detection of single molecule unbinding (Ros et al. 1998; Fuhrmann and Ros 2010). Prior to the experiment one binding partner is immobilized to the sample surface while the other is coupled to the cantilever via a flexible linker (cf. Fig. 1a). The latter enhances steric flexibility and supports proper complexation. In a typical dynamic force spectroscopy (DFS) experiment, the cantilever is lowered to the surface (cf. Fig. 1b-1). Due to a "contact" between the tip and the sample surface, the cantilever is bent upwards until a certain preassigned force is reached (cf. Fig. 1b-2). Receptor and ligand may recognize each other and form a complex during this contact time. Afterwards, the cantilever is retracted from the surface at constant velocity (cf. Fig. 1b-3). The linker molecules and the receptor-ligand-complex are stretched and the corresponding force is imposed on the cantilever (cf. Fig. 1b-4). The slope of the non-linear force ramp is referred to as effective spring constant k_{eff}, i.e., the elasticity of cantilever, linker, and receptor ligand complex. If the externally applied force exceeds the bond strength, the receptor-ligand complex dissociates and the cantilever snaps back to its original zero position. The dissociation force F_{u} and the molecular elasticity k_{eff} at the point of dissociation can be easily derived from the force distance plot (cf. Fig. 1b). As these dissociation events are of stochastic nature this experiment has to be repeated many times to gain the most probable dissociation force F_{max}.

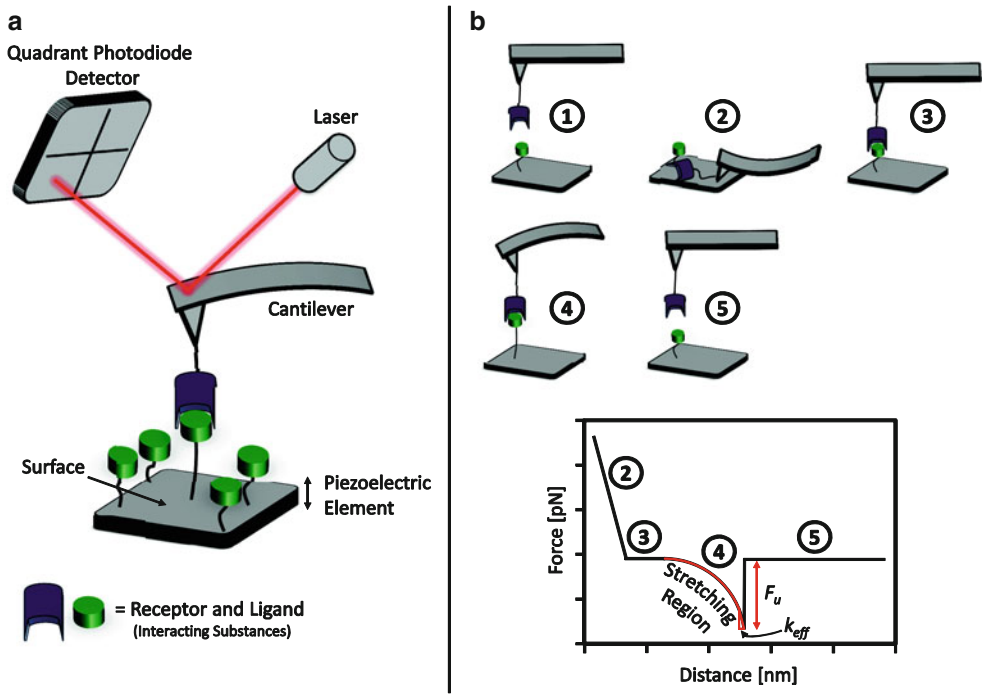

Fig. 1 Schematic representation of a single-molecule force spectroscopy setup and a typical force-distance curve. **a** Two interacting molecules can be immobilized on the surface and the cantilever tip, respectively. A piezoelectric element safeguards a very accurate vertical movement of the surface. Due to the stretching of the molecules a force is imposed on the cantilever resulting in a bending of the flexible element. A laser beam is reflected by the cantilever on a quadrant photodiode. Every movement of the cantilever results in a change of the position of the laser spot on the detector. **b** Different stages of a force spectroscopy measurement: *1* the cantilever approaches the surface. *2* Contact between the tip of the cantilever and the surface results in an upward bending of the flexible element. The ligand interacts with the receptor during this contact time. *3* Afterwards, the cantilever is withdrawn from the surface. *4* Due to the stretching of the linker molecules and the receptor–ligand complex, the cantilever deflects. *5* The receptor–ligand complex dissociates. The step height corresponds to the dissociation force F_{u} while the slope directly before the rupture is related to the molecular elasticity k_{eff}

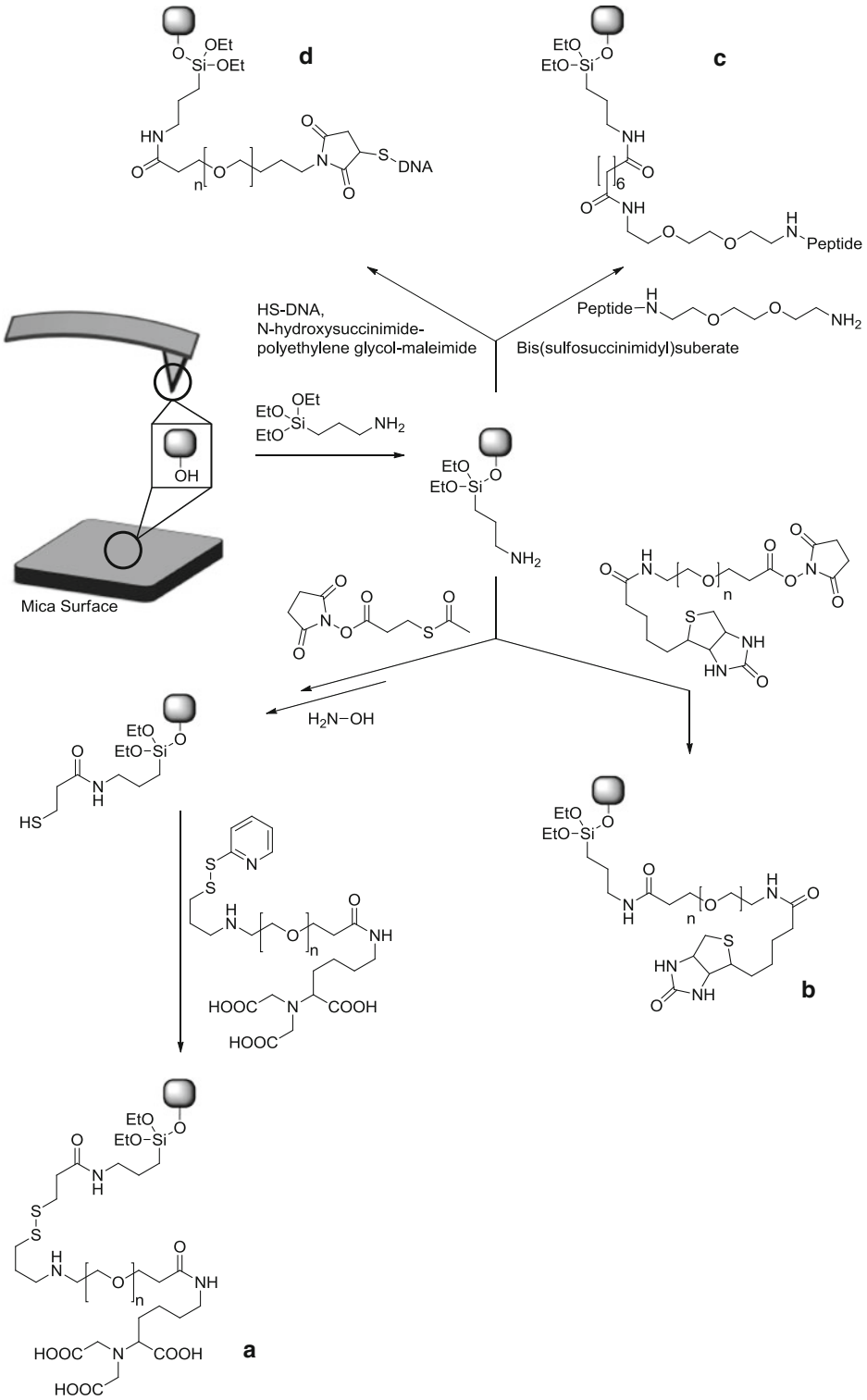

Fig. 2 Different immobilization techniques used in single-molecule force spectroscopy. After silanization of the mica surface or the cantilever using aminopropyltriethoxysilane different NHS-ester derivatives can be used for further modification. **a** Derivatization with *N*-succinimidyl-*S*-acetylthiopropionate (SATP) followed by cleavage of the *S*-acetyl groups with hydroxylamine and the subsequent addition of PDP–PEG–NTA results in a nitrilotriacetic acid modified surface. **b** Biotin–PEG–NHS-active ester enables the immobilization of streptavidin labeled compounds. **c** Amines can easily be immobilized using bis(sulfosuccinimidyl)suberate. Corresponding peptides are accessible by SPPS using 2-chlorotrityl resin loaded with the C-terminal linker 3,6-dioxa-1,8-diaminooctane. **d** *N*-hydroxysuccinimide–polyethylene glycol-maleimides enable the immobilization of thiol modified compounds like oligonucleotides

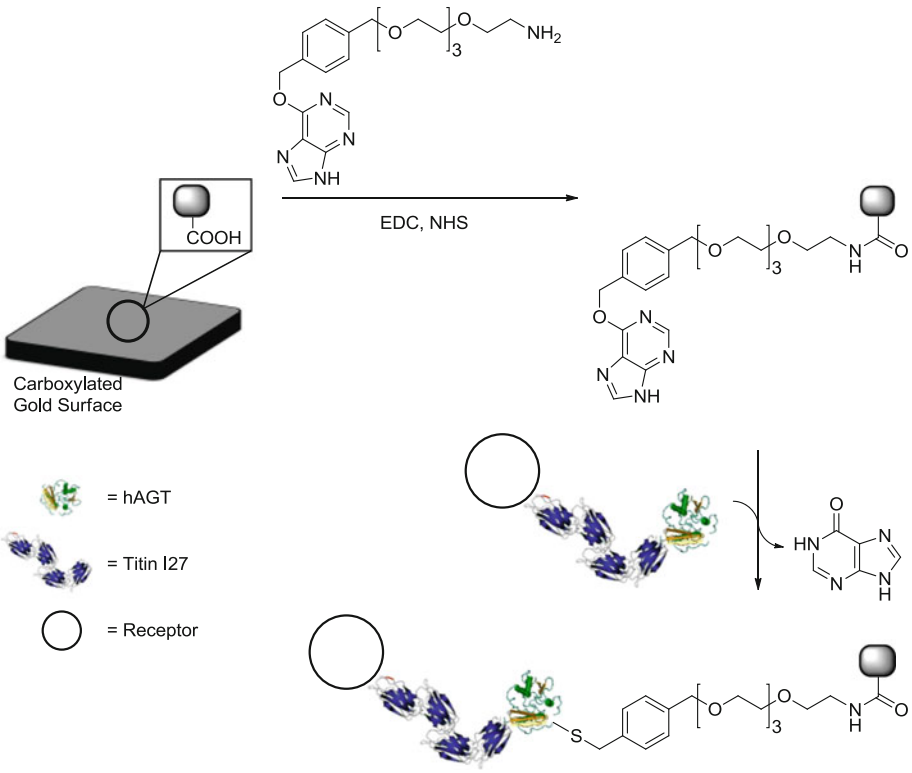

Fig. 3 A fusion protein consisting of the receptor of interest, titin I27 and the O^6-alkylguanine-DNA-alkyltransferase (hAGT) is overexpressed. Addition of the crude cell extract to a carboxylated gold surface derivatized with a benzylguanine–PEG-amino derivative results in the covalent immobilization of the receptor

Immobilization chemistry

Immobilization of the interacting partners on the tip of the cantilever and the surface is a crucial step for the accuracy and reliability of the data. Biomolecules like proteins or DNA molecules can easily be immobilized on unmodified surfaces through hydrophobic or electrostatic interactions (Rief et al. 1999; Younes-Metzler et al. 2011). However, the interaction between the surface and the sample is not stable and often leads to exchange events. Furthermore, multi-oriented immobilization and the possibility that the protein might denature on the surface are disadvantages of this technique (Ferretti et al. 2000). A second method is the complexation of Ni–NTA by a hexahistidine–tag (cf. Fig. 2a). Using this method peptides and proteins were successfully coupled to the tip of a cantilever and immobilized on a mica surface (Andre et al. 2007; Liu et al. 2008; Riener et al. 2003). Another type of non-covalent immobilization method involves the biotin-streptavidin or avidin-streptavidin interaction (cf. Fig. 2b) since it is the strongest non-covalent interaction ($K_a = 10^{15}\ M^{-1}$) in nature (Green 1963). However, the biotin–streptavidin interaction contributes to the elastic response of the whole system and has, therefore, to be taken into consideration during the evaluation (Florin et al. 1994; Smith et al. 1996). The most versatile immobilization methods employ covalent chemistry, because all rupture events detected are exclusively those of the interaction partners. Due to the formation of stable sulfur–gold bonds, a direct covalent attachment of thiol-containing compounds is possible. In this context, intein-mediated protein splicing followed by native chemical ligation with cysteine is an elegant way to modify proteins that lack a cysteine residue (Rief et al. 1998; Wollschläger et al. 2009). The direct immobilization of thiol-modified oligonucleotides on gold surfaces is also possible (Hegner et al. 1993; Lynch et al. 2009). However, in the case of commercially obtained thiol-functionalized DNA it has to be taken into consideration that compounds like dithiothreitol (DTT) used to cleave the dimethoxytrityl protection group (DMT) might still be present in the sample. These compounds can lead to a reduced amount of surface-bound DNA and should be removed before immobilization (Lee et al. 2005). Further techniques for the covalent immobilization are based on heterobifunctional cross-linkers. Linkers in general have the advantage that they minimize interference from interactions with the surface. If they are extensively characterized, they enable the differentiation between pulling an ensemble of molecules instead of a single one due to their contribution to the stretching part of the force–distance curve. Especially PEG-based linkers feature a rich stretching profile in water (Oesterhelt et al. 1999). One well-characterized linker for the immobilization of thiol-modified DNA molecules is the already mentioned *N*-hydroxysuccinimide–polyethylene glycol-maleimide that exhibits an average length of 30 nm (Hinterdorfer et al. 1996; Eckel et al. 2005). After

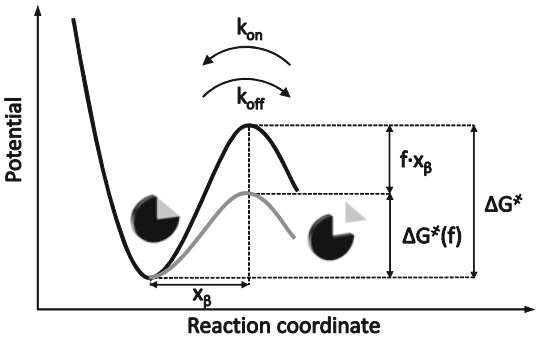

Fig. 4 The bound and unbound states are separated by a potential barrier ($\Delta G^{\neq}$). The corresponding rate constants are k_{on} for the complex formation and k_{off} for the dissociation and the reaction length is x_β. An external force (f), reduces the energy of the transition state. Due to the new, lower potential barrier ($\Delta G^{\neq}(f)$) dissociation events occur more often

silanization of the mica surface with aminopropyltriethoxysilane the PEG-derivative cross-links the modified surface with the oligonucleotide (cf. Fig. 2d). A similar linker approach for peptides is based on the solid-phase peptide synthesis (SPPS) of the corresponding ligand using a 2-chlorotrityl resin loaded with the C-terminal linker 3,6-dioxa-1,8-diaminooctane (cf. Fig. 2c). Immobilizing the peptides on the modified mica surface can then be achieved using bis(sulfosuccinimidyl)suberate (Eckel et al. 2005; Wollschläger et al. 2009). Both strategies are applicable for the surface and also for the cantilever preparation.

Another approach is based on a clickable PEG-linker that was used to click an azide-functionalized antiricin antibody to a gold-coated AFM tip (Chen et al. 2009). Instead of PEG-based cross-linkers the well-characterized oligomer of titin I27 and the protein of interest can be overexpressed as a fusion protein. If only one receptor molecule interacts with the corresponding ligand during the force-spectroscopy measurement the titin I27-based linker undergoes characteristic transitions at 65 pN (Steward et al. 2002). Carboxymethylamylose is a polymer linker for protein and DNA immobilization. Kühner et al. immobilized the polymer on amino-silanized mica surface and cantilever using *N*-hydroxysuccinimide and EDC. Subsequent addition of amino-modified oligonucleotides or proteins resulted in a covalent immobilization. Notably, the authors checked the reliability of their immobilization chemistry by fluorescence spectroscopy using a Cy5 labeled protein and Cy3 labeled DNA. Due to the protein–DNA interaction, a fluorescence resonance energy transfer (FRET) was detectable (Kühner et al. 2004). By combining the titin I27 approach with an enzyme-based immobilization reaction, Kufer et al. developed a procedure to immobilize proteins for single-molecule force spectroscopy directly from crude cell extracts (cf. Fig. 3). The method is based on the expression of a fusion protein consisting of the receptor of interest, titin I27 and the O^6-alkylguanine-DNA-alkyltransferase (hAGT). Addition of the crude cell extract to a carboxylated gold surface derivatized with a benzylguanine–PEG-amino derivative results in the covalent attachment of the fusion protein (Kufer et al. 2005).

Evaluation of the single-molecule spectroscopy data

A variety of parameters that give insight into the binding strength and flexibility of the investigated interaction can be extracted from the results of the single-molecule force spectroscopy experiment. The force imposed on the cantilever is calculated from its deflection using Hooke's law:

$$F = -kd \tag{1}$$

where F is the force, k the spring constant, and d the deflection. The cantilever stiffness depends on various parameters like material properties, dimensions, and shape. Due to minor variations in the production process or chemical modification the spring constant can vary significantly even within the same batch. Hence, it is essential to calibrate the cantilever properly prior to the experiment. Calibration methods can be divided into four major groups: (1) Comparing the new cantilever with a cantilever of known stiffness (Cumpson et al. 2004). (2) Regarding the shift of the resonant frequency after attaching an added end mass to the cantilever (Cleveland et al. 1993). (3) Calculation of the spring constant after estimating the cantilever's dimensions and resonant frequency (Sader et al. 1995). (4) Measuring the cantilever's thermal fluctuation to calculate the effective spring constant (Hutter and Bechhoefer 1993). While all methods exhibit an accuracy of $\sim$10 % the latter is used most common. As it is non-destructive, it can be applied to readily modified cantilevers and it is implemented in most commercial AFM-control software packages.

Extracting the information regarding the strength of the interaction

The basic framework of single-molecule force spectroscopy that consistently bridges macroscopic ensemble parameters and nanoscopic force data was worked out by Evans and Ritchie (1997) who based their work on the path leading publications of Bell (1978) and Kramers (1940). In the following the derivation of the Kramers-Bell-Evans model is sketched briefly: An interaction between a receptor (R) and a ligand (L) results in the corresponding complex (RL). In thermal equilibrium the rates of association and dissociation k^0_{on} and k^0_{off} are constant (cf. Fig. 4).

$$L + R \underset{k_{off}^0}{\overset{k_{on}^0}{\rightleftharpoons}} RL. \tag{2}$$

As the interactions are weak, thermal fluctuations can drive the system to overcome the free activation barrier $(\Delta G^{\neq})$. Hence, according to Kramers rate theory (Kramers 1940), the dissociation rate constant can be written as follows:

$$k_{off}^0 \propto \exp\left(-\frac{\Delta G^{\neq}}{k_B T}\right) \tag{3}$$

with k_B being the Boltzmann constant and T the temperature. Application of an external force lowers the potential barrier by the quantity fx_β:

$$\Delta G^{\neq}(f) = G^{\neq} - fx_\beta \tag{4}$$

with f being the externally applied force and x_β the distance between the potential minimum and the maximum of the potential barrier (reaction length) (cf. Fig. 4). Equations (3) and (4) result in a force dependent off-rate which is known as Bell rate (Bell 1978):

$$k_{off}(f) = k_{off}^0 \exp\left(-\frac{fx_\beta}{k_B T}\right). \tag{5}$$

The dissociation of a complex can be described as a thermally activated decay governed by reaction kinetics of the form:

$$\frac{dp(t)}{dt} = -k_{off}(f(t))\, p(t) \tag{6}$$

where $p(t)$ is the probability that the bond is intact at time t. As the molecular relaxation is much faster than the temporal evolution of the force, the dissociation of the complex is only governed by the force currently applied, i.e., the evolution of the external force has no impact on $p(t)$. Moreover, re-association can be neglected. In dynamic force spectroscopy assays the cantilever is pulled back at constant velocity (v). Therefore, the cantilever displacement (s) is a function of time:

$$s = vt \tag{7}$$

Hence, the force ($f(t)$) is only affected by the current displacement ($s(t)$) and not by the pulling velocity (v):

$$f(t) = f(vt) = f(s) \tag{8}$$

During SMFS experiments, the force imposed on the complex is directly measured by the cantilever deflection and is well known. Therefore, to solve Eq. (6) the time has to be substituted by force $(dt \rightarrow df)$:

$$df = \frac{df}{dx}\frac{dx}{dt}dt = k_{eff}\, v\, dt \tag{9}$$

with k_{eff} and v being the effective elasticity and the pulling velocity, respectively. The product of k_{eff} and v is commonly referred to as loading rate r. After substitution and solving Eq. (6) $p(f)$ results in

$$\rho_v(f) = \exp\left[-\frac{k_{off}}{r}\frac{\exp\left(\frac{x_\beta f}{k_B T}\right) - \exp\left(\frac{x_\beta f_{min}}{k_B T}\right)}{\frac{x_\beta f}{k_B T}}\right]. \tag{10}$$

The theoretical probability distribution of the dissociation forces—in the experimental part referred to as force histogram—is the negative force derivation of Eq. (10) corresponding to $-\frac{dp(f)}{df}$. In the final step the most probable dissociation force F_{max} is linked with the (thermodynamic) dissociation rate constant k_{off}. This is done by estimating the peak of the predicted force distribution: Solving the second force derivation of Eq. (10) for zero force, results in the expression derived by Strunz et al. (2000):

$$F_{max} = \frac{k_B T}{x_\beta}\ln\left(\frac{x_\beta\, r}{k_{off}^0\, k_B T}\right). \tag{11}$$

The most probable dissociation forces increase proportionally to $\ln(r)$ (i.e., higher pulling velocities). Consequently, to get a good estimate for k_{off} and x_β it is essential to run the experiment at numerous pulling velocities preferably spanning several orders of magnitude. Apart from numerical approximation of Eq. (11) to the data, k_{off} and x_β can also be determined ad-hoc by plotting the maximum dissociation forces semi-logarithmically versus the loading rates (Strunz et al. 2000). As the data lie on a straight line it can be expressed by a linear equation $y(x) = mx + b$. Thus, Eq. (11) has to be rewritten accordingly. Now, the potential binding length can be estimated by $x_\beta = \frac{k_B T}{m}$ and k_{off} from the y axis intersection $b = r\frac{x_\beta}{k_B T}$. Another value beside the dissociation rate constant k_{off} and the reaction length x_β that

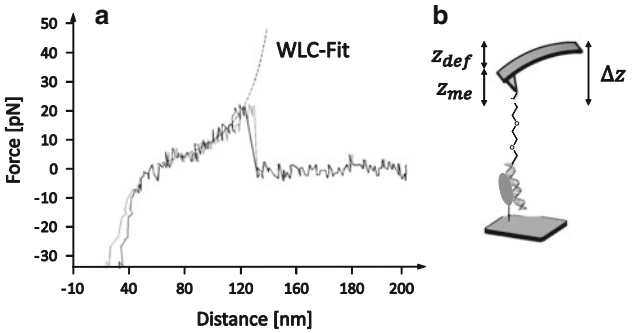

Fig. 5 **a** Force–distance curves before (*gray curve*) and after the correction for the molecular extension (*black curve*). To describe the elasticity of the polymer models like the wormlike chain model (WLC) can be fitted to the stretching region. **b** Schematic representation of the difference between the deflection (z_{def}) and the molecular elongation (z_{me}) that both contribute to the total displacement (Δz)

is always connected with the interaction strength of a complex is its lifetime τ that approximates the inverse dissociation rate constant:

$$\tau = \frac{1}{k_{\text{off}}^0}. \tag{12}$$

In contrast to ensemble methods where the stochastic nature of unbinding events is tackled by ensemble averaging, single-molecule experiments have to be repeated frequent times to get an exact approximation of the unbinding force distribution (Wollschläger et al. 2009).

Although SMFS has proven to be a valuable tool and the results are supported by complementary methods, there are slight inconsistencies that are still being discussed (Evstigneev and Reimann 2003). The probability of the survival of the complex should be independent from the pulling velocity. Hence, plotting the probability against the force for different retract velocities should result in a single master curve. However, in the case of the interaction between the regulatory protein ExpG and its cognate DNA sequence the functions do not converge to a single curve but exhibit a disagreement by two orders of magnitude (Raible et al. 2004). A comparable problem was shown in the case of a micropipette-based force probe setup (Nguyen-Duong et al. 2003). The possible reasons for the fluctuations might be random variations of the surrounding molecules like ions or solvent molecules, different conformations of the interacting partners due to thermal activation, orientational fluctuations of the investigated complex with respect to the applied pulling force or the appearance of unspecific rupture events (Raible et al. 2006). Therefore, the statistical fluctuations of the repetitions of the experiments are accounted for in another approach called heterogeneous bond model. The fluctuations of the dissociation length x_β are approximated using a truncated Gaussian distribution:

$$p(\alpha; a, \sigma) = \exp\left(-\frac{(\alpha - a)^2}{2\sigma^2}\right)\Theta(\alpha) \tag{13}$$

with $p(\alpha; a, \sigma)$ being the corresponding probability distribution, $\alpha = \frac{x_\beta}{k_B T}$ and a and σ being the average and the standard deviation of α, respectively. Moreover, deviations concerning the dissociation rate constant without applying an external force $\left(k_{off}^0\right)$ are included into the heterogeneous bond model. The ansatz based on the postulation of heterogeneities of the chemical bonds in extension of the standard theory results in a good agreement of theoretically calculated and experimentally measured data (Raible et al. 2006).

Extracting the contour, persistent and Kuhn lengths of the polymer

The region of the force–distance curve preceding the rupture point is also called stretching region (cf. Figs. 1, 5a) as the slope of the force curve is the effective spring constant of the whole system (cf. Fig. 5b), i.e., cantilever, linkers, and receptor ligand complex. To gain an insight into the elastic properties of the stretched molecules the displacement Δz (cantilever travel, cf. Fig. 5a gray curve) has to be corrected for the molecular extension z_{me}, i.e., the elongation of the molecules (cf. Fig. 5a black curve) (Cappella and Dietler 1999):

$$z_{\text{me}} = \Delta z - z_{\text{def}} \tag{14}$$

where z_{def} is the deflection of the cantilever in nanometers.

Depending on the applied force a differentiation between entropic and enthalpic elasticity is necessary. Models can be fitted to the stretching region to describe entropic elasticity of a polymer. The freely jointed chain model (FJC) is based on the idea that a polymer consists of N rigid subunits that are freely able to rotate (Smith et al. 1996):

$$x(F) = L\left(\coth\left(\frac{Fb}{k_B T}\right) - \frac{k_B T}{Fb}\right). \tag{15}$$

Thereby x is the end-to-end length, F the applied force, L the contour length $(L = Nb)$ and b the Kuhn length (length of each segment). Alternatively, the wormlike chain model (WLC) treats the polymer as a homogeneous, flexible rod (cf. Fig. 5a):

$$F(x) = \frac{k_B T}{l}\left(\frac{1}{4\left(1 - \frac{x}{L}\right)^2} - \frac{1}{4} + \frac{x}{L}\right). \tag{16}$$

Here, l is the persistence length (the distance along which the molecule can be considered as rigid) (Bouchiat et al. 1999). If the applied force is increased (above 5–10 pN for DNA) the elasticity becomes increasingly enthalpic due to the fact that the polymer backbone is stretched and bond-angles are deformed (Odijk 1995). In that case, an extended form of both models has to be used. To include stiffness of the chain into the WLC model the elastic modulus (Φ) is introduced (Wang et al. 1997):

$$F(x) = \frac{k_B T}{l}\left(\frac{1}{4\left(1 - \frac{x}{L} + \frac{F(x)}{\Phi}\right)^2}\frac{F(x)}{\Phi} - \frac{1}{4} + \frac{x}{L}\right). \tag{17}$$

This new parameter measures the intrinsic resistance to longitudinal strain of the polymer and thereby reflects enthalpic contributions.

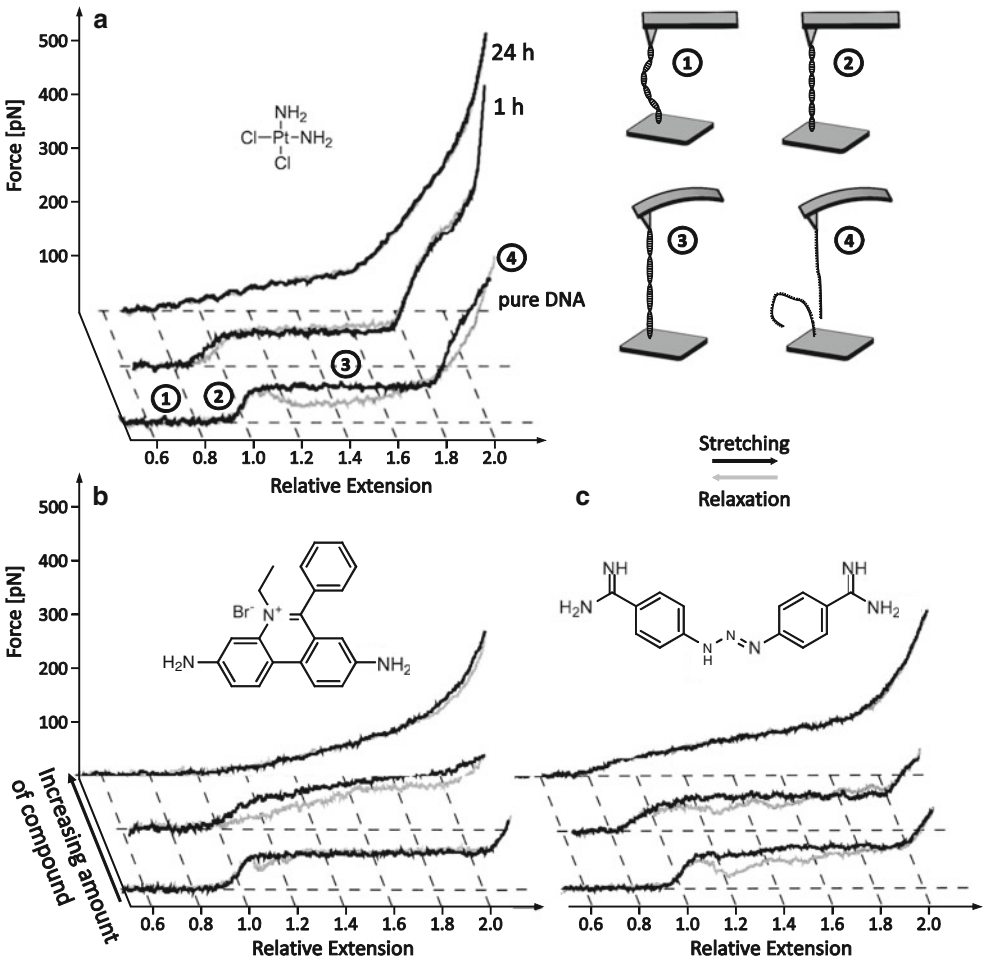

Fig. 6 A double-stranded DNA molecule is stretched between AFM-tip and surface in the presence of different concentrations of cisplatin (**a**), ethidium bromide (**b**) and berenil (**c**) (results from Krautbauer et al. 2000, 2002). The *black curves* correspond to the elongation, whereas the *gray ones* refer to the relaxation. **a** Elongating the pure DNA molecule (*1* + *2*) results in the formation of a plateau at approximately 65 pN in the force–extension curve due to an overstretched DNA molecule to >170 % of the B-DNA contour length (*3*). Finally, the double-stranded helix starts to melt (*4*). In the presence of cisplatin, progress of the DNA recognition by the compound was followed after 1 and 24 h. The hysteresis of the stretching and relaxation has vanished indicating that cisplatin inhibits the separation of the two DNA strands. **b** Increasing the ethidium bromide amount up to 1 molecule per 2 bp leads to a shortening of the overstretching plateau due to the unwinding and stretching of the DNA. **c** Increasing the amount of berenil up to 1 molecule per 4 bp only leads to minor deviations. However, a further increase up to 1 molecule per 0.4 bp leads to a drastic change and a curve similar to the one of ethidium bromide

Dynamic force spectroscopy of protein/peptide-DNA interactions

Intercalation and DNA-recognition by small molecules

The first investigation of the mechanical properties of oligonucleotides using an AFM-based single-molecule force spectroscopy setup was performed by Rief et al. (1999). Stretching DNA molecules results in a distinct plateau (cf. Fig. 6a) due to a highly cooperative B–S transition of the oligonucleotide, where S is an overstretched conformation that exhibits approximately 170 % of the contour length of the B-DNA. Of note, this transition was recently ascertained as partial melting of basepairs (van Mameren et al. 2009). The force value of the transition depends on the sequence and on experimental properties like the buffer composition (Wenner et al. 2002). Further stretching finally results in two separated single strands (cf. Fig. 6a). The corresponding relaxation trace (cf. Fig. 6, grey curve) does not resemble the stretching curve. At lower forces, approximately below 150 pN, partial melting of the double-stranded DNA may occur resulting in a deviation of the relaxation trace from the stretching curve. This melting hysteresis indicates that a force-induced melting occurred (Krautbauer et al. 2002).

Small molecules interacting with the DNA influence the stretching mechanics of oligonucleotides. Krautbauer et al. used AFM-based single-force spectroscopy to investigate structural changes of the DNA induced by cisplatin

(Krautbauer et al. 2000). Cisplatin interacts preferentially with N7 atoms of guanine bases of DNA by forming cross-links in the oligonucleotide. Intrastrand cross-linked bases can either be neighboring or separated by any other base. The authors stretched platinated DNA molecules with varying base compositions and compared the mechanical properties of untreated and treated oligonucleotides. All results indicate that cisplatin inhibits a permanent mechanical separation of the duplex since the relaxation traces are indistinguishable from the extension traces even at high forces (cf. Fig. 6a). Moreover, DNA-molecules that contain guanine bases exhibit a faster re-annealing process due to the platination. Cisplatin, therefore, seems to stabilize the double-stranded structure. The authors extended their investigation in 2002 by comparing the mechanical behavior of oligonucleotides incubated with the minor groove binder berenil, the cross-linker cisplatin, and the intercalator ethidium bromide to be able to distinguish between different modes of binding (Krautbauer et al. 2002).

Every molecule showed a characteristic pattern in the corresponding force–distance curves. Cisplatin induces shortening of the oligonucleotide and the complete loss of melting hysteresis as described above (cf. Fig. 6a). The cross-linker increases the force-range of the overstretching process. Ethidium bromide induces unwinding and stretching of the DNA molecule resulting in the observed shortened transition (cf. Fig. 6b). Still, the necessity to apply higher forces at the end of the transition shows that the DNA is partially stabilized by the intercalator. The aromatic di-amidine berenil only affects the low-force region (cf. Fig. 6c). At high concentrations the resulting force–distance curve exhibits similarities with the one of ethidium bromide suggesting an additional intercalating mechanism.

Furthermore, we investigated the intercalators daunomycin, ethidium bromide and YO, and the bis-intercalant YOYO using an analogous setup (Eckel et al. 2003; Ros et al. 2004). Bis-intercalation mode was shown to enforce the effects of typical intercalators.

Two other intercalators that were investigated by single-molecule force spectroscopy are the aromatic compounds acridine and pyrene (Jiang et al. 2010; Liu et al. 2007). In both cases the interaction with oligonucleotides was investigated directly by immobilizing the DNA molecule on the surface and the corresponding intercalator on the tip of the cantilever. Liu et al. reported that the most probable rupture force of the acridine intercalation depends on the loading rate and, therefore, suggested a dynamic recognition process (Liu et al. 2007). Jiang et al. analyzed the interaction of pyrene and oligonucleotides with and without mismatches (Jiang et al. 2010). Significant differences were detected that enable the identification of oligonucleotides with mismatches. Both intercalators exhibit a comparable most probable rupture force of approximately 36 pN at a loading rate of 5.0 nN s^{-1}.

DNA-aptamers

Aptamers are single-stranded DNA molecules that specifically interact with target molecules due to their intrinsic secondary structure (Liu et al. 2009). Thiolated DNA-aptamers were immobilized on the tip of a cantilever by Basnar et al. (2006). Although the interaction between the aptamer and thrombin was detectable, only a very low force of 4.45 pN was measured. This value seems to correspond to the melting force of the aptamer. Using the same pair of interacting molecules but with an inverted setup, Yu et al. detected stronger interactions due to the avoidance of sterical problems (Yu et al. 2007). Neundlinger et al. applied an enhanced linker design by immobilizing the biotinylated DNA-aptamers on PEG-streptavidin functionalized tips (Neundlinger et al. 2011). Another approach for the immobilization of aptamers was published by Zhang et al. (Zhang and Yadavalli 2011). The authors used thiolated aptamers and oligoethylene glycol thiols to create self-assembled monolayers, thereby preventing nonspecific protein adsorption on the tip surface. Using this immobilization procedure the interaction between the DNA-aptamer and the two target proteins immunoglobulin E and the vascular endothelial growth factor (VEGF) was successfully quantified.

Interaction between DNA and peptides

We investigated the recognition of poly(dG-dC) dsDNA by peptides comprising the sequence Ac-(Leu-Ala-Arg-Leu)$_3$-NH-Linker and Ac-(Aib-Leu-Arg)$_4$-NH-linker (Eckel et al. 2003).

The design of the peptides is based on the sequence Ac-(Leu-Ala-Arg-Leu)$_x$-NHMe (x = 1–4), which exhibits amphiphilic properties and is known for its gene-transfer abilities (Lee et al. 1986). Moreover, every peptide comprises the C-terminal linker 3,6-dioxa-1,8-diaminooctane, that was introduced by solid-phase peptide synthesis. The first peptide is characterized by an α-helical structure, whereas the second one features a 3_{10}-helical conformation. All side chains of the latter are arranged in a collinear manner due to the fact that the peptide possesses three amino acids per turn (Sewald et al. 2006). Stretching of the double-stranded DNA in the presence and the absence of both peptides and comparing these results with force-distance curves recorded in the presence of the minor groove binder distamycin A and different intercalators revealed that the interaction mechanism of both peptides with the DNA differs (cf. Fig. 7). These findings support the

assumption that the peptides bind to the major groove of the oligonucleotide (Eckel et al. 2003).

A 20 amino acid residue epitope of the bacterial transcription activator PhoB was immobilized on the tip of the cantilever and the corresponding cognate DNA sequence on a mica surface to further investigate the recognition of specific DNA sequences by synthetic peptides (Eckel et al. 2005). Circular dichroism spectroscopy measurements revealed that the peptide exhibits a high tendency to form a helix. Using this setup we were able to determine the dissociation rate constant of the peptide–DNA complex with a value of $k_{\mathrm{off}} = (3.1 \pm 2.1)\,\mathrm{s}^{-1}$ and the molecular reaction length with a value of $x_\beta = (6.8 \pm 1.2)$ Å. Competition experiments using either the oligonucleotide or the peptide as competitor in a huge excess were performed to validate the sequence specificity of the binding process. In both cases the data indicate a significant decrease in total binding probability (cf. Fig. 8b). Washing the cantilever and the surface with pure buffer and repeating the experiment resulted in a complete recovery of the primary interaction (cf. Fig. 8c). Moreover, certain amino acids that are known to be involved in the interaction with the DNA sequence were substituted by alanine. Performing single-molecule force spectroscopy experiments with these point mutants facilitated the investigation of the contribution of the corresponding residues to the overall recognition process.

Recognition of DNA by proteins

The first site-specific single-molecule force spectroscopy characterization of a protein–DNA interaction using an AFM-based setup was performed by Bartels et al. (Bartels et al. 2003; Anselmetti et al. 2008). The transcriptional activator ExpG from *Sinorhizobium meliloti* is involved in the galactoglucan biosynthesis. Binding of the protein to three different DNA sequences comprising the recognition site was investigated. Therefore, the protein of interest was immobilized on a silanized mica surface using the cross-linker bis(sulfosuccinimidyl) suberate. The corresponding thiol-modified oligonucleotides were ligated to the silanized cantilever tips using *N*-hydroxysuccinimide-poly(ethylene glycol)-maleimide. Using this setup, dissociation rate constants in the range of $k_{\mathrm{off}} = (1.2 \pm 1.0) \times 10^{-3}\mathrm{s}^{-1}$ corresponding to lifetimes of about 830 s and a reaction length of $x_\beta = (7.5 \pm 1.0)$Å could be derived for all DNA molecules. In the datasets of the loading-rate dependent measurements two regions can be distinguished (cf. Fig. 9). In the lower loading rate region all protein-DNA complexes share the same slope under a linear fit. However, in the higher loading rate region above 11,000 pN s^{-1}, widely varying slopes can be found. The corresponding reaction lengths range from $x_\beta = (0.39 \pm 0.14)$Å to $x_\beta = (2.0 \pm 0.6)$Å. One explanation for this divergent behavior is a second energy barrier in all systems that exhibit different properties with respect to the DNA sequences.

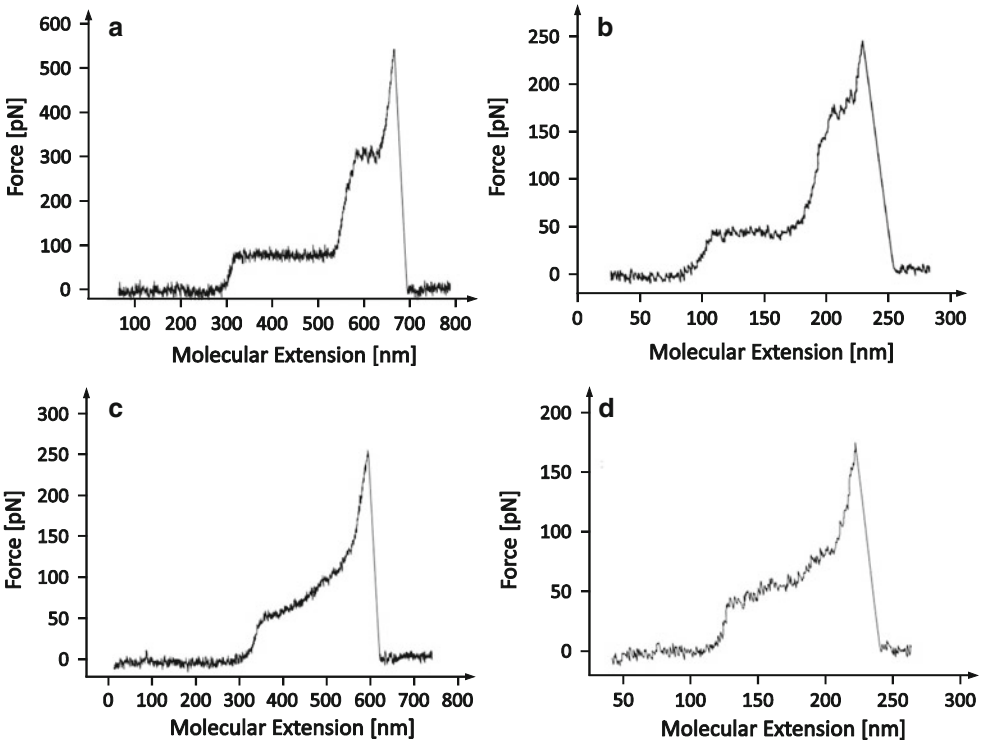

Fig. 7 Force–extension curves of poly(dG-dC) dsDNA in the absence (**a**) and in the presence of distamycin A (**b**) and the major groove binding α-helical (**c**) and 3_{10}-helical (**d**) peptides (Results from Eckel et al. 2005). Comparing all results reveals that the binding mode of the minor groove binder distamycin A (**b**) differs from the one of the two peptides (**c**, **d**). We concluded from these findings that the peptides address the major groove

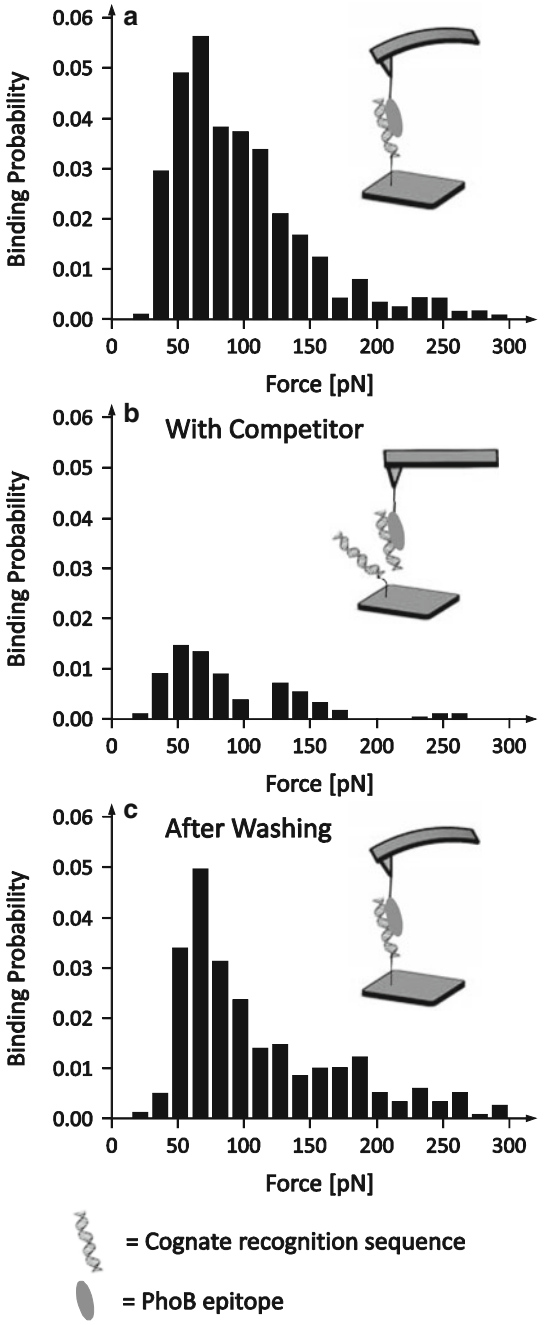

Fig. 8 Competition experiments using a synthetic PhoB epitope immobilized on the tip of the cantilever, the corresponding cognate DNA recognition sequence immobilized on a mica surface and the same oligonucleotide as competitor (Results from Eckel et al. 2005). **a** Force histogram of the single-force spectroscopy measurement without competitor. **b** Using an excess of competitor significantly reduces the binding probability. This result proves that the recognition of the DNA molecule by the synthetic epitope is sequence specific. **c** Removing the competitor in a washing step results in the recovery of the specific recognition of the immobilized DNA sequence

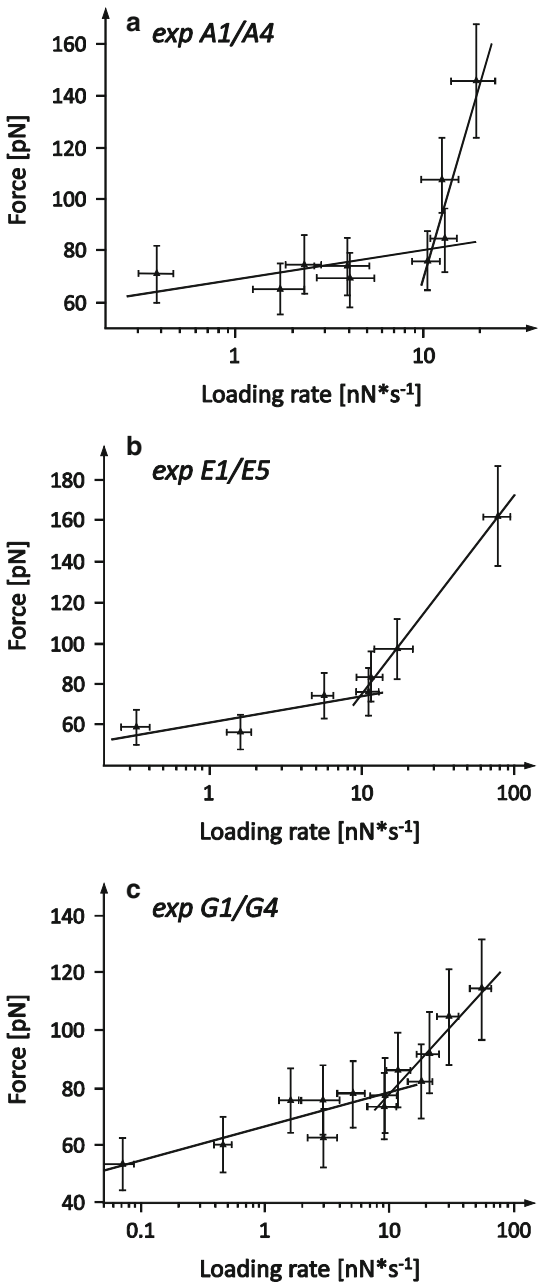

Fig. 9 Loading rate dependent force measurements of the interaction between the transcriptional activator ExpG and three different oligonucleotides (*exp A1/A4*, *E1/E5* and *G1/G4*) comprising the recognition site of the protein (data from Bartels et al. 2003). All three complexes exhibit the same slope at low loading rates. However, at high loading rates, the slope shows differences in consequence of a second energy barrier that depends on the oligonucleotide sequence

Point mutations were inserted into the promoter to further analyze the significance of different regions of the recognition sequence of ExpG and binding of the transcriptional activator to the corresponding oligonucleotides was investigated (Baumgarth et al. 2005). The contribution of different promoter regions to the overall binding process was determined.

Another system that has also been investigated by AFM-based single-molecule force spectroscopy is LexA (Kühner

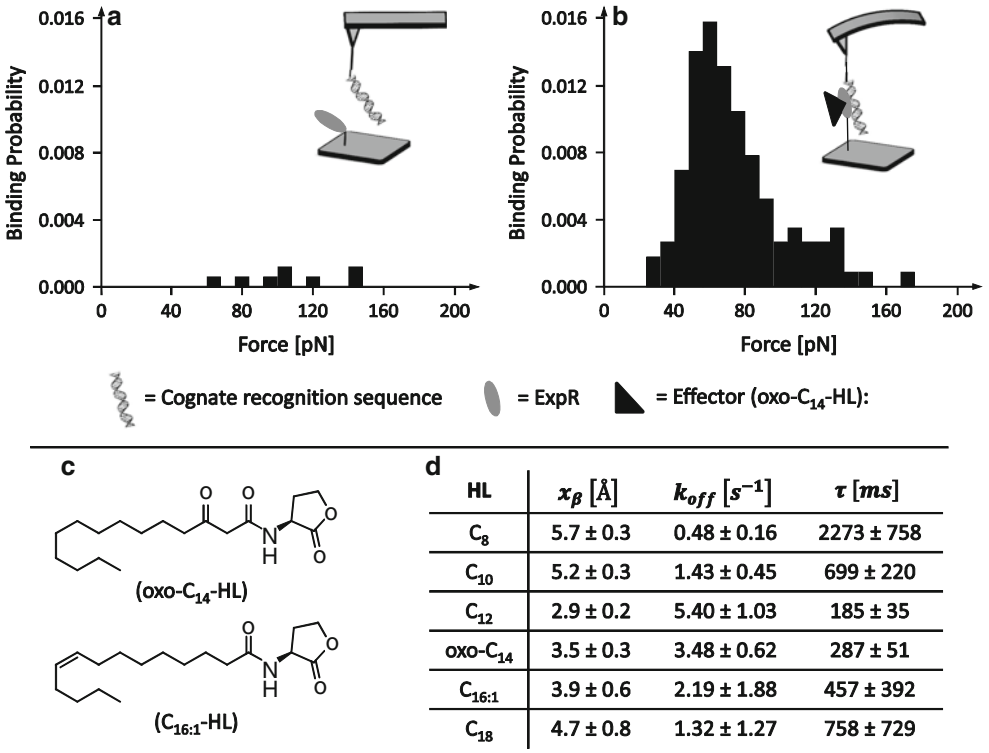

HL	x_β [Å]	k_{off} [s^{-1}]	τ [ms]
C_8	5.7 ± 0.3	0.48 ± 0.16	2273 ± 758
C_{10}	5.2 ± 0.3	1.43 ± 0.45	699 ± 220
C_{12}	2.9 ± 0.2	5.40 ± 1.03	185 ± 35
oxo-C_{14}	3.5 ± 0.3	3.48 ± 0.62	287 ± 51
$C_{16:1}$	3.9 ± 0.6	2.19 ± 1.88	457 ± 392
C_{18}	4.7 ± 0.8	1.32 ± 1.27	758 ± 729

Fig. 10 Force spectroscopy measurements of the interaction between the transcriptional activator ExpR and the *sinRI* locus in the presence and the absence of *N*-acyl homoserine lactones (AHLs) (data from Bartels et al. 2007). **a** Force histogram recorded without any effector present. **b** Force histogram recorded after the addition of oxo-C_{14}-HL. **c** Structure of the two AHLs with modifications in the acyl side chain: *N*-(3-Oxotetradecanoyl)-*L*-homoserine lactone (oxo-C_{14}-HL) and *N*-[(9Z)-hexadec-9-enoyl]-*L*-homoserine lactone ($C_{16:1}$-HL). **d** Summary of the reaction lengths (x_β) dissociation rate constants (k_{off}) and lifetimes (τ) of the ExpR-DNA complex in the presence of different AHLs

et al. 2004). The repressor protein controls approximately 31 genes involved in the SOS system of *Escherichia coli* (*E. coli*) and binds to its palindromic recognition sequence as a dimer. As described above, the authors introduced carboxymethylamylose as linker for the protein and DNA immobilization. A Cy3–Cy5 based FRET assay was performed to validate the applied immobilization method. Moreover, the interaction between the oligonucleotide and the carboxymethylamylose was investigated by performing an experiment with the fully functionalized tip and a mica surface that lacks LexA to exclude unspecific interactions. For the two operons *recA* and *yebG* dissociation rate constants of $k_{off} = 0.045\,s^{-1}$ and $k_{off} = 0.13\,s^{-1}$ were measured, respectively. The corresponding short-range widths of the binding potentials with values of $x_\beta = (5.1 \pm 1.0)$Å and $x_\beta = (4.9 \pm 0.5)$Å, respectively, are characteristic for a stiff hydrogen-bonding network.

Another important topic that has been investigated using single-molecule force spectroscopy is the impact of certain effector molecules on protein–DNA interactions (Bartels et al. 2007). Bacterial quorum sensing allows the coordination of gene expression with respect to the population

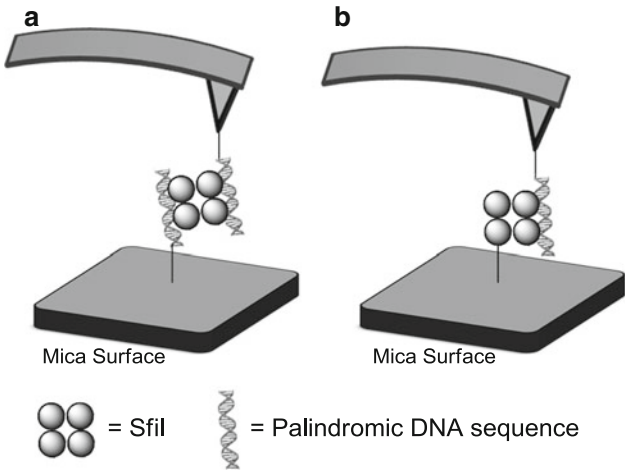

Fig. 11 Schematic representation of the two investigation approaches to analyze the interaction between the restriction enzyme SfiI and the corresponding palindromic DNA sequence (Krasnoslobodtsev et al. 2007). **a** The palindromic sequence was immobilized on the mica surface and on the tip of the cantilever followed by the addition of the homotetrameric protein to investigate the synaptic complex. **b** Immobilizing the restriction enzyme on a mica surface and the corresponding DNA sequence on the tip of the cantilever enables the biophysical characterization of the pre-synaptic complex

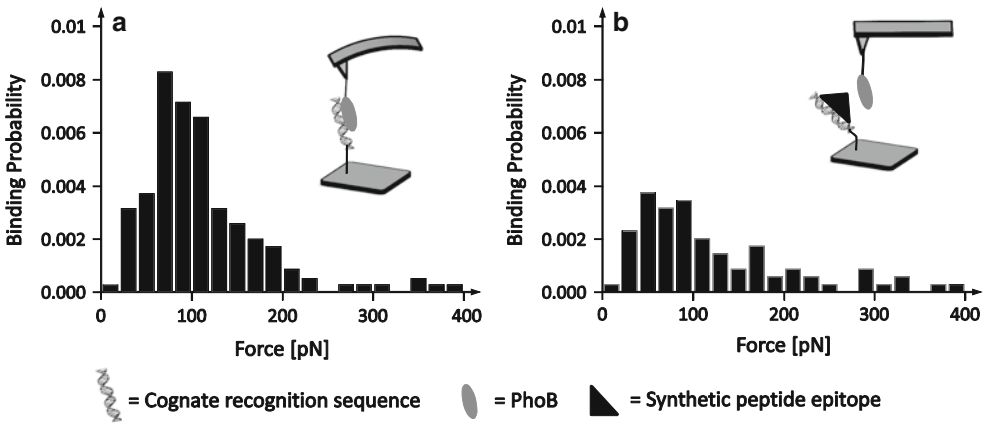

c

Mutation	Protein (PhoB 127-229)		Peptide (PhoB 190-209)	
	$k_{off}\ [s^{-1}]$	$\tau\ [s]$	$k_{off}\ [s^{-1}]$	$\tau\ [s]$
WT	0.0025 ± 0.0021	400	3.1 ± 2.1	0.32
R193A	0.012 ± 0.008	83	0.071 ± 0.053	14
H198A	0.76 ± 0.25	0.020	50 ± 21	0.020
R203A	----	----	----	----
R176A	1.9 ± 1.2	0.53		
T217A	0.53 ± 0.20	1.87		
V218A	0.14 ± 0.35	6.98		
Y223A	0.45 ± 0.32	2.21		

Fig. 12 **a**, **b** Competition experiments using the complete DNA-binding domain of PhoB (PhoB 127–229) immobilized on the tip of the cantilever and the corresponding cognate DNA recognition sequence immobilized on a mica surface. Addition of a 25-fold excess of the synthetic PhoB epitope (PhoB 190–209) results in a 55 % overall decrease of binding (**b**) (results from Wollschläger et al. 2009). **c** Summary of the results from single-molecule force spectroscopy measurements using the cognate recognition sequence of PhoB and different point mutants of the entire DNA binding domain (PhoB 127–229) and of a synthetic epitope (PhoB 190–209) (results from Wollschläger et al. 2009 and Ritzefeld et al. 2013)

density. Small effector molecules like *N*-acyl homoserine lactones (AHLs) that readily cross the bacterial cell wall accumulate intracellularly and extracellularly and activate LuxR-type transcriptional regulators if a certain threshold is reached (reviewed by Fuqua et al. 2001). The effect of different AHLs on the recognition of the *sinRI* locus by the transcriptional activator ExpR from *Sinorhizobium meliloti* was investigated (Bartels et al. 2007). Without any effector molecule present the formation of the protein–DNA complex is nearly completely suppressed (cf. Fig. 10a). However, the addition of *N*-(3-oxotetradecanoyl)-*L*-homoserine lactone (oxo-C_{14}-HL) results in a significantly increased binding probability (cf. Fig. 10b). Moreover, investigations on the impact of different AHLs revealed that the averaged lifetime of the protein-DNA complex and the corresponding reaction length seem to depend on the chain length and the structure of the effector compound (cf. Fig. 10d). These results support the hypothesis that ExpR regulates the corresponding target genes differently in response to different AHLs.

The SfiI is a restriction enzyme that was analyzed by AFM based force spectroscopy. It forms homotetramers and recognizes the palindromic sequence

$$5' - GGCCNNNN \downarrow NGGCC - 3' \quad (17)$$

where ↓ indicates the cleavage site (Krasnoslobodtsev et al. 2007). Normally, magnesium is required as cofactor. However, exchanging magnesium by calcium leads to stable SfiI-DNA complexes that are not cleaved. The SfiI tetramer can form either a synaptic complex with two duplexes or a pre-synaptic complex consisting of one duplex and the protein. The authors used two approaches to investigate both types of interaction. In the first setup, 13 bp dsDNA molecules comprising the recognition sequence were immobilized on the tip of the cantilever and also on the mica surface (cf. Fig. 11a). Addition of the restriction enzyme to the system results in the formation of the synaptic complex consisting of SfiI and the two DNA molecules. Due to the symmetry of the complex, both duplexes can dissociate when a force is applied. A second

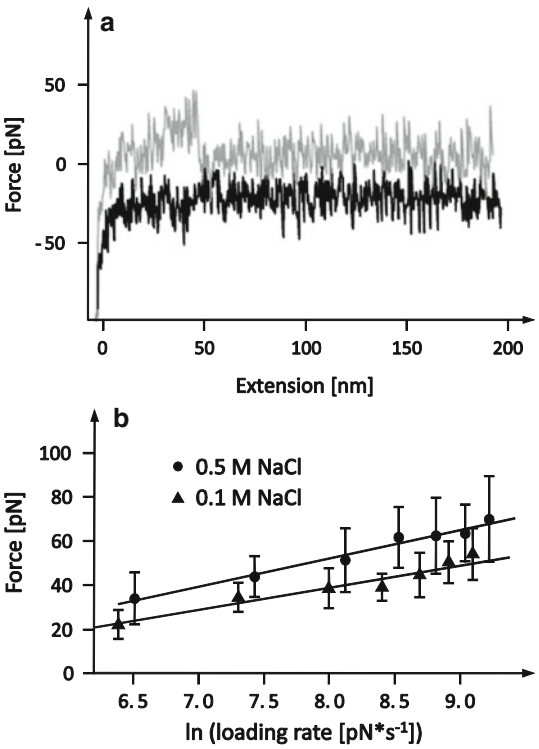

Fig. 13 **a** Typical force–extension curve for SSB–ssDNA complexes (Results from Zhang et al. 2011). The *black curve* corresponds to the cantilever approaching the surface and the *grey one* is recorded during the retraction. **b** Most probable rupture forces of the SSB-ssDNA recorded at different salt concentrations (0.5 and 0.1 M NaCl) are plotted logarithmically against the loading rates. Using linear regression a reaction length of $x_\beta = 0.41$ nm and a dissociation off-rate constant of ($k_{\text{off}} = 6.91\ \text{s}^{-1}$) in the presence of 0.1 M NaCl and a reaction length of $x_\beta = 0.34$ nm and a dissociation off-rate constant of $k_{\text{off}} = 4.11\ \text{s}^{-1}$ in the presence of 0.5 M NaCl could be derived

setup based on the standard approach where the oligonucleotide is immobilized on the tip of the cantilever and the protein of interest on the mica surface was used to analyze the pre-synaptic complex (cf. Fig. 11b). Comparison of the results of both setups revealed that the pre-synaptic and the synaptic complex are characterized by a comparable rupture force. Moreover, the authors investigated the contribution of the central region of the palindromic recognition sequence by analyzing binding of SfiI to three oligonucleotides. The corresponding dissociation rate constants with values of $k_{\text{off}} = 38\,\text{s}^{-1}(5' - TCGA \downarrow G - 3')$, $k_{\text{off}} = 70\,\text{s}^{-1}(5' - AAAC \downarrow A - 3')$ and $k_{\text{off}} = 248\text{s}^{-1}(5' - AAAA \downarrow A - 3')$, are in good agreement with the spacer effect on the SfiI catalytic activity.

The transcription activator PhoB induces the expression of approximately 31 genes involved in the phosphate metabolism of *E. coli*. Beside the investigated peptide epitopes described above (Eckel et al. 2005) binding of the complete DNA-binding domain of PhoB to the corresponding recognition sequence was analyzed on the single-molecule level (Wollschläger et al. 2009). Competition experiments were performed by adding a 25-fold excess of the synthetic peptide to the protein–DNA complex and repeating the force spectroscopy measurements. The results indicate that binding of the entire DNA binding domain—PhoB(DBD)—to the cognate recognition sequence is stronger and more specific than binding of the peptide epitope to the oligonucleotide (cf. Fig. 12a, b). Still, the addition of the peptide resulted in a 55 % overall decrease of binding. Alanine mutants of PhoB(DBD) were obtained by site-directed mutagenesis to verify amino acid residues known to be involved in the DNA interaction. Comparison of the force spectroscopy results of the mutant proteins with the data of the synthetic epitopes indicates the same tendency in nearly all cases (cf. Fig. 12c). Thus, the contributions of certain single amino acid residues to the molecular recognition process on the protein and peptide level were identified.

Site-directed mutagenesis was employed on the protein level (cf. Fig. 12c) to discriminate between different binding types involved in the protein–DNA interaction in surface plasmon resonance (SPR) and AFM-based force spectroscopy studies (Ritzefeld et al. 2013). Single-molecule methods facilitate a more accurate differentiation of the amino acid contribution, whereas SPR additionally enables the investigation of effects based on protein–protein interactions. By applying both techniques and correlating the results with X ray and NMR structural analysis the contributions of electrostatic interactions with narrow minor grooves, interactions mediated by hydrogen bonding and stabilizing effects due to protein–protein interactions to the overall recognition process could be distinguished.

Chromatin is a complex of DNA compacted around the core histone octamer that consists of two copies of the proteins H2A, H2B, H3, and H4. Interactions between multiple histones result in the formation of a 30-nm chromatin fiber which is further packed by non-histone proteins into a higher order chromosome structure (Luger et al. 1997). Soni et al. immobilized chromatin on an APTES-glutaraldehyde (AP-GD)-coated mica surface, located a single octamer using the results obtained from AFM imaging and investigated the rupture force profile of the dissociation of the individual histone complex (Soni et al. 2007). The authors extracted the most probable rupture force with a value of approximately 51 pN at a loading rate of 10^{-7} N s^{-1}. This value is larger than the force required to disrupt the nucleosome core particle DNA complex indicating that the protein–protein interactions stabilizing the chromatin fiber are stronger than the corresponding protein–DNA interactions. Hameed et al. investigated the differences between chromatin isolated from normal and apoptotic cells (Hameed et al. 2009). The authors transfected the enhanced green fluorescent protein (EGFP)-tagged

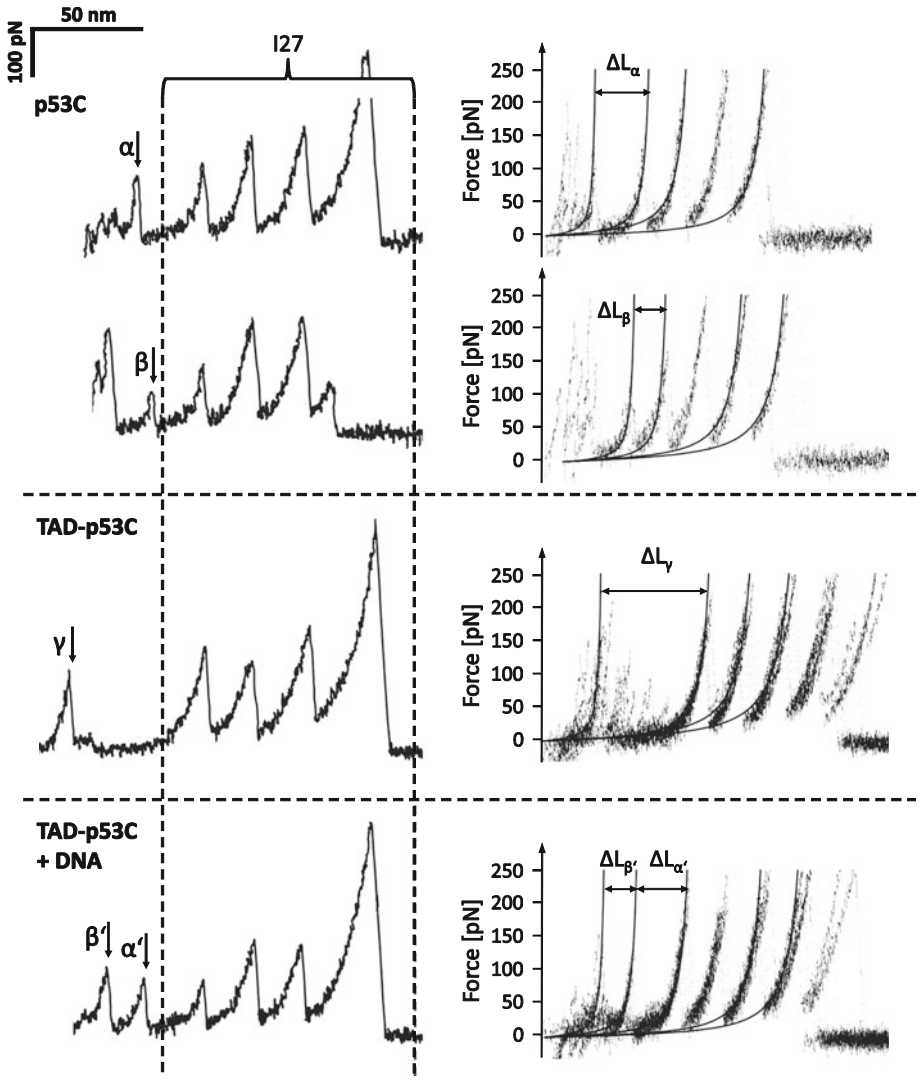

Fig. 14 The mechanical unfolding trajectory of p53C-I27 and TAD-p53C-I27 fusion proteins in the absence and presence of an oligonucleotide comprising the p53 recognition sequence (Results from Taniguchi and Kawakami 2012). The force–extension curves of the fusion proteins on the left side exhibit unfolding peaks characteristic for certain unfolding events (labeled with α, β, γ, α′ and β′), whereas the last four peaks refer to the unfolding of the I27 domains. On the *right side* superimposed traces of the related force extension curves are shown. *Solid lines* are fits using the WLC model. The contour length increment were estimated to be $\Delta L_\alpha = 34 \pm 1$ nm, $\Delta L_\beta = 22 \pm 3$ nm, $\Delta L_\gamma = 76 \pm 3$ nm, $\Delta L_{\alpha'} = 35 \pm 1$ nm and $\Delta L_{\beta'} = 21 \pm 3$ nm

histone H2B into HeLa cells and purified the supernatant of the lysed cells using a fluorescence-activated cell sorter. Afterwards the chromatin was covalently immobilized using an AP-GD coated mica surface. An AP-GD coated cantilever tip was lowered into the chromatin to covalently attach the complex to the tip, too. During the retraction of the cantilever, multiple disruptions were detected that correspond to various different interactions in between the fibers. The authors extracted the effective spring constant of the cantilever–chromatin complex from these curves and compared the distribution of the probability of the corresponding values of chromatin derived from normal cells with the probability distribution of chromatin derived from apoptotic cells. The most probable value for the chromatin stiffness of normal cells was estimated to be $k_{\mathrm{ch\_N}} = 4\mathrm{pN\ nM^{-1}}$ and the corresponding value for the chromatin stiffness of apoptotic cells $k_{\mathrm{ch\_Ap}} = 1\mathrm{pN\ nM^{-1}}$. These results indicate that the chromatin from apoptotic cells exhibits a reduced stiffness due to modifications of the chromatin structure.

Single-stranded DNA-binding proteins (SSB) form another class of proteins investigated using AFM-based single-molecule force spectroscopy. Zhang et al. determined the unbinding force of complexes consisting of SSB proteins derived from *Bacillus subtilis* and single-stranded oligonucleotides at different salt concentrations (cf. Fig. 13a) (Zhang et al. 2011). The protein was ligated to the silicon substrate and the single-stranded oligonucleotide to the tip of the cantilever using the typical maleimide PEG cross-linker based immobilization chemistry. This setup enabled the assignment of specific interactions by determining the corresponding rupture length. Control experiments without the ssDNA or the protein were performed to further validate the specificity of the interaction. The authors derived a reaction length of $x_\beta = 0.41$ nm and a dissociation off-rate constant of $k_{\mathrm{off}} = 6.91\ \mathrm{s^{-1}}$ in the

presence of 0.1 M NaCl from the recorded data (cf. Fig. 13b). Increasing the salt concentration to 0.5 M NaCl results in a reduced reaction length $x_\beta = 0.34$ nm and a higher off-rate constant ($k_{off} = 4.11\ s^{-1}$) indicating that a more tightly packed SSB-ssDNA complex is formed in a 0.5-M NaCl solution.

The tetrameric tumor suppressor protein p53 consists of four identical chains each comprising an N-terminal transactivation domain (TAD), followed by a proline-rich region (PRR), the central DNA-binding domain (p53C), the tetramerization domain (TET), and the extreme C terminus (CT). p53 regulates several cellular processes like DNA repair, apoptosis, and the cell cycle. Remarkably, more than 50 % of all human tumors exhibit a mutation or deletion of the TP53 gene (Joerger and Fersht 2008). Taniguchi and Kawakami used nonspecific protein-cantilever and protein mica-surface interactions to mechanically unfold one fusion protein consisting of p53's DNA-binding domain sandwiched by titin I27 domains and another fusion protein that additionally contains the TAD domain in the absence and presence of DNA (Taniguchi and Kawakami 2012). The retract phase of every force peak was fitted using the WLC model. Moreover, the last four force peaks in all extension traces correspond to the unfolding of the I27 domains and were therefore used as fingerprint for the fusion protein (cf. Fig. 14). Unfolding the p53C results in at least two patterns of force profiles with contour length increments of $\Delta L_\alpha = 34 \pm 1$ nm and $\Delta L_\beta = 22 \pm 3$ nm (cf. Fig. 14). However, the results also indicate that there are at least two distinct pathways in the mechanical unfolding of the protein. In the case of the TAD-p53C fusion protein a high frequency of force peaks with a contour length increment of $\Delta L_\gamma = 76 \pm 3$ nm could be detected indicating the unfolding of a domain consisting of 220 amino acids. Due to the fact that the p53C domain exhibits 199 amino acids, these results reveal that the DNA-binding domain does not solely unfold. Addition of an oligonucleotide comprising the p53 consensus sequence to the TAD-p53C fusion protein results in a different force profile. Two consecutive force peaks with contour lengths at $\Delta L_{\beta'} = 21 \pm 3$ nm and $\Delta L_{\alpha'} = 35 \pm 1$ nm were detected. Hence, the unfolding events are in good agreement with the contour lengths detected for the pure p53C. However, only a single unfolding pathway dominates (cf. Fig. 14). In conclusion, the DNA alters the mechanical stability of the DNA-binding domain and presumably stabilizes a residual structure during the unfolding process.

Conclusions

During the past two decades AFM-based single-molecule force spectroscopy was successfully applied to a broad range of different DNA interactions. The relationship between macroscopic parameters and nano-mechanic properties is accomplished on the basis of the Kramers-Bell-Evans Model. Despite the discussion concerning minor modifications or extensions of this model, this approach has proven its validity in an overwhelming number of experiments not merely in the investigation of DNA–Protein interactions but in the whole (non-covalent) supramolecular interplay (Jarchow et al. 2000; Schäfer et al. 2007; Fuhrmann et al. 2009; Schroeder et al. 2012). A wide variety of sophisticated immobilization strategies have been developed that allow for the elucidation of intermolecular interactions at the single-molecule level. Due to the superior sensitivity only small amounts of analyte are needed. Furthermore, elaborate synthesis techniques enable to produce custom-tailored molecules and, therefore, selectively address, analyze, and quantify specific molecular interactions.

Apart from thermodynamics and kinetics, SMFS also provides an insight into the intermolecular energy landscape. As the reaction length is proportional to the inverse slope of the force vs. loading rate plot, non-constant gradients indicate complex binding energy landscapes. In particular, the high dynamic range of AFM-based SMFS allows to explore these more complex potentials and enable the identification and investigation of binding mechanisms.

Moreover, SMFS is a suitable method to explore multifaceted binding mechanisms like catch-bonds that are found in adhesion proteins that are discussed elsewhere (not discussed here). Catch-bonds behave un-intuitively as they become more stable in certain loading force regimes. Most likely allosteric effects and/or changes of the molecular conformation are responsible for this (Thomas et al. 2008).

With growing complexity of the interested system, it is increasingly demanding to extract the desired information from the force data. Despite the wide range of commercially available AFM hard-, software and accessories, the successful implementation and interpretation of SMFS experiments still demand substantial knowledge and experience. Furthermore, the serial measurement of single dissociation events needs the recurring repetition of force distance cycles to gain a sufficient amount of data. This and the thorough analysis of thousands of force curves requires considerably more time than ensemble experiments. In contrast to other SMFS techniques like optical or magnetic tweezers, AFM also has limited force resolution making it difficult to observe certain protein (un-) folding processes. Nevertheless, this issue can be tackled, e.g., with low noise detectors (Schäffer et al. 2000) in combination with small cantilevers (Bustamante et al. 2000; Viani et al. 1999).

Summing up, various custom-tailored synthesis and sample preparation procedures, the ability to conduct measurements under near-physiological conditions and the

possibility to measure forces with piconewton (pN) resolution at a wide dynamic range makes AFM-based SMFS an indispensable method for the elucidation of DNA interactions.

References

Andre G, Brasseur R, Dufrêne YF (2007) Probing the interaction forces between hydrophobic peptides and supported lipid bilayers using AFM. J Mol Recognit 20:538–545. doi:10.1002/jmr.837

Anselmetti D, Bartels FW, Becker A et al (2008) Reverse engineering of an affinity-switchable molecular interaction characterized by atomic force microscopy single-molecule force spectroscopy. Langmuir 24:1365–1370. doi:10.1021/la702373b

Ashkin A, Dziedzic JM (1987) Optical trapping and manipulation of viruses and bacteria. Science 235:1517–1520. doi:10.1126/science.3547653

Bartels FW, Baumgarth B, Anselmetti D et al (2003) Specific binding of the regulatory protein ExpG to promoter regions of the galactoglucan biosynthesis gene cluster of Sinorhizobium meliloti—a combined molecular biology and force spectroscopy investigation. J Struct Biol 143:145–152. doi:10.1016/S1047-8477(03)00127-8

Bartels FW, McIntosh M, Fuhrmann A et al (2007) Effector-stimulated single molecule protein-DNA interactions of a quorum-sensing system in sinorhizobium meliloti. Biophys J 92:4391–4400. doi:10.1529/biophysj.106.082016

Basnar B, Elnathan R, Willner I (2006) Following aptamer—thrombin binding by force measurements. Anal Chem 78:3638–3642. doi:10.1021/ac052289e

Baumgarth B, Bartels FW, Anselmetti D et al (2005) Detailed studies of the binding mechanism of the Sinorhizobium meliloti transcriptional activator ExpG to DNA. Microbiology 151:259–268. doi:10.1099/mic.0.27442-0

Bell GI (1978) Models for the specific adhesion of cells to cells. Science 200:618–627

Binnig G, Quate CF, Gerber C (1986) Atomic force microscope. Phys Rev Lett 56:930–933. doi:10.1103/PhysRevLett.56.930

Bouchiat C, Wang MD, Allemand J et al (1999) Estimating the persistence length of a worm-like chain molecule from force-extension measurements. Biophys J 76:409–413. doi:10.1016/S0006-3495(99)77207-3

Bustamante C, Macosko JC, Wuite GJL (2000) Grabbing the cat by the tail: manipulating molecules one by one. Nat Rev Mol Cell Biol 1:130–136. doi:10.1038/35040072

Cappella B, Dietler G (1999) Force-distance curves by atomic force microscopy. Surf Sci Rep 34:5–104. doi:10.1016/S0167-5729(99)00003-5

Chen G, Ning X, Park B et al (2009) Simple, clickable protocol for atomic force microscopy tip modification and its application for trace ricin detection by recognition imaging. Langmuir 25:2860–2864. doi:10.1021/la803523b

Cleveland JP, Manne S, Bocek D, Hansma PK (1993) A nondestructive method for determining the spring constant of cantilevers for scanning force microscopy. Rev Sci Instrum 64:403–405. doi:10.1063/1.1144209

Cumpson PJPJ, Zhdan P, Hedley J (2004) Calibration of AFM cantilever stiffness: a microfabricated array of reflective springs. Ultramicroscopy 100:241–251. doi:10.1016/j.ultramic.2003.10.005

Dammer U, Popescu O, Wagner P et al (1995) Binding strength between cell adhesion proteoglycans measured by atomic force microscopy. Science 267:1173–1175. doi:10.1126/science.7855599

Drake B, Prater CB, Weisenhorn AL et al (1989) Imaging crystals, polymers, and processes in water with the atomic force microscope. Science 243:1586–1589. doi:10.1126/science.2928794

Eckel R, Ros R, Ros A et al (2003) Identification of binding mechanisms in single molecule—DNA complexes. Biophys J 85:1968–1973. doi:10.1016/S0006-3495(03)74624-4

Eckel R, Wilking SD, Becker A et al (2005) Single-molecule experiments in synthetic biology: an approach to the affinity ranking of DNA-binding peptides. Angew Chem Int Ed 44:3921–3924. doi:10.1002/anie.200500152

Evans E, Ritchie K (1997) Dynamic strength of molecular adhesion bonds. Biophys J 72:1541–1555. doi:10.1016/S0006-3495(97)78802-7

Evstigneev M, Reimann P (2003) Dynamic force spectroscopy: optimized data analysis. Phys Rev E Stat Nonlin Soft Matter Phys 68:045103. doi:10.1103/PhysRevE.68.045103

Ferretti S, Paynter S, Russell DA et al (2000) Self-assembled monolayers: a versatile tool for the formulation of bio-surfaces. TrAC Trends Anal Chem 19:530–540. doi:10.1016/S0165-9936(00)00032-7

Florin EL, Moy VT, Gaub HE (1994) Adhesion forces between individual ligand-receptor pairs. Science 264:415–417. doi:10.1126/science.8153628

Fuhrmann A, Ros R (2010) Single-molecule force spectroscopy: a method for quantitative analysis of ligand–receptor interactions. Nanomedicine 5:657–666. doi:10.2217/nnm.10.26

Fuhrmann A, Schoening JC, Anselmetti D et al (2009) Quantitative analysis of single-molecule RNA-protein interaction. Biophys J 96:5030–5039. doi:10.1016/j.bpj.2009.03.022

Fuqua C, Parsek MR, Greenberg EP (2001) Regulation of gene expression by cell-to-cell communication: acyl-homoserine lactone quorum sensing. Annu Rev Genet 35:439–468. doi:10.1146/annurev.genet.35.102401.090913

Gosse C, Croquette V (2002) Magnetic tweezers: micromanipulation and force measurement at the molecular level. Biophys J 82:3314–3329. doi:10.1016/S0006-3495(02)75672-5

Green NM (1963) Avidin. 3. The nature of the biotin-binding site. Biochem J 89:599–609

Hameed FM, Soni GV, Krishnamurthy H, Shivashankar GV (2009) Probing structural stability of chromatin assembly sorted from living cells. Biochem Biophys Res Commun 385:518–522. doi:10.1016/j.bbrc.2009.05.086

Hegner M, Wagner P, Semenza G (1993) Immobilizing DNA on gold via thiol modification for atomic force microscopy imaging in buffer solutions. FEBS Lett 336:452–456. doi:10.1016/0014-5793(93)80854-N

Hinterdorfer P, Baumgartner W, Gruber HJ et al (1996) Detection and localization of individual antibody-antigen recognition events by atomic force microscopy. Proc Natl Acad Sci USA 93:3477–3481. doi:10.1073/pnas.93.8.3477

Hutter JL, Bechhoefer J (1993) Calibration of atomic-force microscope tips. Rev Sci Instrum 64:1868–1873. doi:10.1063/1.1143970

Jarchow J, Fritz J, Anselmetti D et al (2000) Supramolecular structure of a new family of circular proteoglycans mediating cell adhesion in sponges. J Struct Biol 132:95–105. doi:10.1006/jsbi.2000.4309

Jiang Z, Zhang Y, Yu Y et al (2010) Study on intercalations between double-stranded DNA and pyrene by single-molecule force spectroscopy: toward the detection of mismatch in DNA. Langmuir 26:13773–13777. doi:10.1021/la102647p

Joerger AC, Fersht AR (2008) Structural biology of the tumor suppressor p53. Annu Rev Biochem 77:557–582. doi:10.1146/annurev.biochem.77.060806.091238

Kramers H (1940) Brownian motion in a field of force and the diffusion model of chemical reactions. Physica 7:284–304. doi:10.1016/S0031-8914(40)90098-2

Krasnoslobodtsev AV, Shlyakhtenko LS, Lyubchenko YL (2007) Probing interactions within the synaptic DNA-SfiI complex by AFM force spectroscopy. J Mol Biol 365:1407–1416. doi:10.1016/j.jmb.2006.10.041

Krautbauer R, Clausen-Schaumann H, Gaub HE (2000) Cisplatin changes the mechanics of single DNA molecules. Angew Chem Int Ed 39:3912–3915. doi:10.1002/1521-3773(20001103)39:21<3912:AID-ANIE3912>3.0.CO;2-5

Krautbauer R, Pope LH, Schrader TE et al (2002) Discriminating small molecule DNA binding modes by single molecule force spectroscopy. FEBS Lett 510:154–158. doi:10.1016/S0014-5793(01)03257-4

Kufer SK, Dietz H, Albrecht C et al (2005) Covalent immobilization of recombinant fusion proteins with hAGT for single molecule force spectroscopy. Eur Biophys J 35:72–78. doi:10.1007/s00249-005-0010-1

Kühner F, Costa LT, Bisch PM et al (2004) LexA-DNA bond strength by single molecule force spectroscopy. Biophys J 87:2683–2690. doi:10.1529/biophysj.104.048868

Lee S, Mihara H, Aoyagi H et al (1986) Relationship between antimicrobial activity and amphiphilic property of basic model peptides. Biochim Biophys Acta 862:211–219. doi:10.1016/0005-2736(86)90485-2

Lee GU, Chrisey LA, Colton RJ (1994) Direct measurement of the forces between complementary strands of DNA. Science 266:771–773. doi:10.1126/science.7973628

Lee C-Y, Canavan HE, Gamble LJ, Castner DG (2005) Evidence of Impurities in Thiolated Single-Stranded DNA Oligomers and Their Effect on DNA Self-Assembly on Gold. Langmuir 21:5134–5141. doi:10.1021/la0472302

Liu C, Jiang Z, Zhang Y et al (2007) Intercalation interactions between dsDNA and acridine studied by single molecule force spectroscopy. Langmuir 23:9140–9142. doi:10.1021/la7013804

Liu Z, Zu Y, Fu Y et al (2008) Assembling and imaging of his-tag green fluorescent protein on mica surfaces studied by atomic force microscopy and fluorescence microscopy. Microsc Res Tech 71:802–809. doi:10.1002/jemt.20622

Liu J, Cao Z, Lu Y (2009) Functional nucleic acid sensors. Chem Rev 109:1948–1998. doi:10.1021/cr030183i

Luger K, Mäder AW, Richmond RK et al (1997) Crystal structure of the nucleosome core particle at 2.8 A resolution. Nature 389:251–260. doi:10.1038/38444

Lynch S, Baker H, Byker SG et al (2009) Single molecule force spectroscopy on G-quadruplex DNA. Chemistry 15:8113–8116. doi:10.1002/chem.200901390

Meyer G, Amer NM (1988) Novel optical approach to atomic force microscopy. Appl Phys Lett 53:1045–1047. doi:10.1063/1.100061

Neundlinger I, Poturnayova A, Karpisova I et al (2011) Characterization of enhanced monovalent and bivalent thrombin DNA aptamer binding using single molecule force spectroscopy. Biophys J 101:1781–1787. doi:10.1016/j.bpj.2011.07.054

Nguyen-Duong M, Koch KW, Merkel R (2003) Surface anchoring reduces the lifetime of single specific bonds. Europhys Lett (EPL) 61:845–851. doi:10.1209/epl/i2003-00311-6

Odijk T (1995) Stiff chains and filaments under tension. Macromolecules 28:7016–7018. doi:10.1021/ma00124a044

Oesterhelt F, Rief M, Gaub HE (1999) Single molecule force spectroscopy by AFM indicates helical structure of poly(ethylene-glycol) in water. New J Phys 6:1–6. doi:10.1088/1367-2630/1/1/006

Raible M, Evstigneev M, Reimann P et al (2004) Theoretical analysis of dynamic force spectroscopy experiments on ligand–receptor complexes. J Biotechnol 112:13–23. doi:10.1016/j.jbiotec.2004.04.017

Raible M, Evstigneev M, Bartels FW et al (2006) Theoretical analysis of single-molecule force spectroscopy experiments: heterogeneity of chemical bonds. Biophys J 90:3851–3864. doi:10.1529/biophysj.105.077099

Ralston J, Larson I, Rutland MW et al (2005) Atomic force microscopy and direct surface force measurements (IUPAC Technical Report). Pure Appl Chem 77:2149–2170. doi:10.1351/pac200577122149

Rief M, Gautel M, Schemmel A, Gaub HE (1998) The mechanical stability of immunoglobulin and fibronectin III domains in the muscle protein titin measured by atomic force microscopy. Biophys J 75:3008–3014. doi:10.1016/S0006-3495(98)77741-0

Rief M, Clausen-Schaumann H, Gaub HE (1999) Sequence-dependent mechanics of single DNA molecules. Nat Struct Mol Biol 6:346–349. doi:10.1038/7582

Riener CK, Kienberger F, Hahn CD et al (2003) Heterobifunctional crosslinkers for tethering single ligand molecules to scanning probes. Anal Chim Acta 497:101–114. doi:10.1016/j.aca.2003.08.041

Ritzefeld M, Sewald N (2012) Real-time analysis of specific protein-DNA interactions with surface plasmon resonance. J Amino Acids 2012:1–19. doi:10.1155/2012/816032

Ritzefeld M, Walhorn V, Kleineberg C et al (2013) Combining Real Time and Single-Molecule Methods to Investigate Protein-DNA Interactions. Submitted

Ros R, Schwesinger F, Anselmetti D et al (1998) Antigen binding forces of individually addressed single-chain Fv antibody molecules. PNAS 95:7402–7405. doi:10.1073/pnas.95.13.7402

Ros R, Eckel R, Bartels F et al (2004) Single molecule force spectroscopy on ligand–DNA complexes: from molecular binding mechanisms to biosensor applications. J Biotechnol 112:5–12. doi:10.1016/j.jbiotec.2004.04.029

Sader JE, Larson I, Mulvaney P, White LR (1995) Method for the calibration of atomic force microscope cantilevers. Rev Sci Instrum 66:3789–3798. doi:10.1063/1.1145439

Schäfer C, Eckel R, Ros R et al (2007) Photochemical single-molecule affinity switch. J Am Chem Soc 129:1488–1489. doi:10.1021/ja067734h

Schäffer TE, Richter M, Viani MB (2000) Array detector for the atomic force microscope. Appl Phys Lett 76:3644–3646. doi:10.1063/1.126734

Schroeder T, Walhorn V, Mattay J, Anselmetti D (2012) Single-molecule force spectroscopy of supramolecular complexes. In: Schalley CA (ed) Analytical methods in supramolecular chemistry. Wiley-VCH, New York, pp 559–606

Sewald N, Wilking SD, Eckel R et al (2006) Probing DNA-peptide interaction forces at the single-molecule level. J Pept Sci 12:836–842. doi:10.1002/psc.820

Shao Z, Yang J, Somlyo AP (1995) Biological atomic force microscopy: from microns to nanometers and beyond. Annu Rev Cell Dev Biol 11:241–265. doi:10.1146/annurev.cb.11.110195.001325

Smith SB, Cui Y, Bustamante C (1996) Overstretching B-DNA: the elastic response of individual double-stranded and single-stranded DNA molecules. Science 271:795–799. doi:10.1126/science.271.5250.795

Soni GV, Brar L, Hameed FM et al (2007) Distinct levels in the nanoscale organization of DNA-histone complex revealed by its mechanical unfolding. Appl Phys Lett 90:163904. doi:10.1063/1.2728031

Steward A, Toca-Herrera JL, Clarke J (2002) Versatile cloning system for construction of multimeric proteins for use in atomic force microscopy. Protein Sci 11:2179–2183. doi:10.1110/ps.0212702

Strunz T, Oroszlan K, Schumakovitch I et al (2000) Model energy landscapes and the force-induced dissociation of ligand-receptor

bonds. Biophys J 79:1206–1212. doi:10.1016/S0006-3495(00)76375-2

Taniguchi Y, Kawakami M (2012) Variation in the mechanical unfolding pathway of p53DBD induced by interaction with p53 N-terminal region or DNA. PLoS ONE 7:e49003. doi:10.1371/journal.pone.0049003

Thomas WE, Vogel V, Sokurenko E (2008) Biophysics of catch bonds. Ann Rev Biophys 37:399–416. doi:10.1146/annurev.biophys.37.032807.125804

van Mameren J, Gross P, Farge G et al (2009) Unraveling the structure of DNA during overstretching by using multicolor, single-molecule fluorescence imaging. PNAS 106:18231–18236. doi:10.1073/pnas.0904322106

Viani MB, Schäffer TE, Chand A et al (1999) Small cantilevers for force spectroscopy of single molecules. J Appl Phys 86:2258. doi:10.1063/1.371039

Wang MD, Yin H, Landick R et al (1997) Stretching DNA with optical tweezers. Biophys J 72:1335–1346. doi:10.1016/S0006-3495(97)78780-0

Wenner JR, Williams MC, Rouzina I, Bloomfield VA (2002) Salt dependence of the elasticity and overstretching transition of single DNA molecules. Biophysical J 82:3160–3169. doi:10.1016/S0006-3495(02)75658-0

Wollschläger K, Gaus K, Körnig A et al (2009) Single-molecule experiments to elucidate the minimal requirement for DNA recognition by transcription factor epitopes. Small 5:484–495. doi:10.1002/smll.200800945

Younes-Metzler O, Ben RN, Giorgi JB (2011) The adsorption of antifreeze glycoprotein fraction 8 on dry and wet mica. Colloids Surf B 82:134–140. doi:10.1016/j.colsurfb.2010.08.029

Yu J, Jiang Y, Ma X et al (2007) Energy landscape of aptamer/protein complexes studied by single-molecule force spectroscopy. Chem Asian J 2:284–289. doi:10.1002/asia.200600230

Zhang X, Yadavalli VK (2011) Surface immobilization of DNA aptamers for biosensing and protein interaction analysis. Biosens Bioelectron 26:3142–3147. doi:10.1016/j.bios.2010.12.012

Zhang W, Lü X, Zhang W, Shen J (2011) EMSA and single-molecule force spectroscopy study of interactions between *Bacillus subtilis* single-stranded DNA-binding protein and single-stranded DNA. Langmuir 27:15008–15015. doi:10.1021/la203752y